Tracking of magnetic helicity evolution in the inner heliosphere

T. Alberti, Y. Narita, L. Z. Hadid, D. Heyner, A. Milillo, C. Plainaki, H.-U. Auster, I. Richter

HAL Id: hal-03774234
https://hal.science/hal-03774234

Submitted on 16 Sep 2022

Tracking of magnetic helicity evolution in the inner heliosphere

A radial alignment study

T. Alberti[1], Y. Narita[2], L. Z. Hadid[3], D. Heyner[4], A. Milillo[1], C. Plainaki[5], H.-U. Auster[4], and I. Richter[4]

[1] INAF-Istituto di Astrofisica e Planetologia Spaziali, via del Fosso del Cavaliere 100, 00133 Roma, Italy, e-mail: `tommaso.alberti@inaf.it`

[2] Space Research Institute, Austrian Academy of Sciences, Schmiedlstr. 6, 8042 Graz, Austria

[3] LPP, CNRS, École Polytechnique, Sorbonne Université, Université Paris-Saclay, Observatoire de Paris, Institut Polytechnique de Paris, PSL Research University, Palaiseau, France

[4] Institut für Geophysik und Extraterrestrische Physik, Technische Universität Braunschweig, Mendelssohnstr. 3, 38106 Braunschweig, Germany

[5] Italian Space Agency, Via del Politecnico, 00133 Roma, Italy.

ABSTRACT

Context. Magnetic helicity is one of the invariants in ideal magnetohydrodynamics, and its spectral evolution has a rich amount of information to reveal the mechanism as to how the space and astrophysical plasmas develop into turbulence.

Aims. The goal of our study is to observationally characterize the magnetic helicity evolution in the inner heliosphere by resolving the helicity transport in a scale-wise fashion in the spectral domain.

Methods. The evolution of magnetic helicity spectrum in the inner heliosphere is tracked using a radial alignment event achieved by Parker Solar Probe at a distance of 0.17 astronomical units from the Sun (hereafter 'au') and BepiColombo at 0.58 AU with a delay of about 3.5 days.

Results. The reduced magnetic helicity resolved in the frequency domain shows three main features: (1) a coherent major peak of highly helical component at the lowest frequency at about 5×10^{-4} Hz, (2) a damping of helicity oscillation at the intermediate frequencies from 10^{-3} to 10^{-2} Hz when observed at 0.58 AU, and (3) a coherent non-helical component in the ion-kinetic range at frequencies of about $0.1 - 1$ Hz.

Conclusions. Though limited in the frequency range, the lesson is that the solar wind develops into turbulence by convecting large-scale helicity components on one hand and creating and annihilating helical wave components on the other hand. Excitation of waves can overwrite the helicity profile in the inner heliosphere. By comparing with the typical helicity spectra at a distance of 1 AU (that is, randomly oscillating helicity sign in the intermediate frequency range up to about 1 Hz), the helicity evolution reaches a nearly asymptotic state at the Venus orbit (about 0.7 au) and beyond.

Key words. magnetic helicity – heliosphere – spacecraft radial alignment

1. Introduction

Understanding the magnetic helicity density $\mathbf{A} \cdot \mathbf{B}$ (hereafter simply the magnetic helicity) and its transport processes in the heliosphere is a likely candidate of breakthrough in the research areas of space and astrophysical plasma turbulence. From the theoretical point of view, the magnetic helicity is an invariant in the ideal magnetohydrodynamic (MHD) system when integrated over the volume bounded by the magnetic surface. The magnetic helicity is considered as an important control or constraint parameter of plasma turbulence such as evolution into helical or non-helical turbulence (Biskamp 2003).

From the observational point of view, on the other hand, proper helicity measurements in space (in particular in the solar wind) remain a challenge. Most of the magnetic field data are provided by the single-point observations, and the helicity study is limited to the analysis of field rotation sense around the radial direction from the Sun assuming Taylor's frozen-in flow hypothesis (Taylor 1938). This makes a marked difference from the numerical simulations in which the magnetic helicity can unambiguously be determined in the spatial domain.

The advent of the inner heliospheric probes performed by Parker Solar Probe, BepiColombo, and Solar Orbiter gives us a variety of observational opportunities by combining the two or three spacecraft data. The evolution or transport process of the magnetic helicity can then be tracked from one region to another. Here we present a radial alignment study of the magnetic helicity from a heliocentric distance of 0.17 AU (below the distance of Mercury's orbit of 0.3 AU) to 0.58 AU (below the distance of Venus' orbit of 0.7 AU). The radial alignment of Parker Solar Probe and BepiColombo was achieved in September 2020 (Alberti et al. 2022). Our helicity study logically extends the helicity evolution study by Telloni et al. (2015) to even closer to the Sun.

Observationally speaking, the outer domain (the Earth orbit and beyond) of heliosphere in the ecliptic plane exhibits a reduced magnetic helicity with (i) random oscillation with zero-mean on the MHD scales up to about 0.1 Hz in the spacecraft frame (Matthaeus et al. 1982; Smith 2003), and (ii) a systematic trend to non-zero value in the ion-kinetic range at about 1 Hz and higher (Leamon et al. 1998; Podesta 2013). The aforementioned observations have undoubtedly contributed in our better understanding of the overall helicity density behavior. However,

the lack of a systematic approach in the analysis of multi-point observations (also due to the design and operations of the related space missions) results in our still limited understanding of the helicity evolution in the inner heliosphere. We address the question if the empirical picture of helicity described above inherits from the helicity profile in the innermost area of heliosphere (below 0.58 AU, previous studies were devoted to larger distances (Telloni et al. 2015)), or if the helicity is actively evolving with generation, dissipation, or transport over different scales.

2. Radial alignment event study

2.1. Data set and analysis

We use measurements provided by the PSP and the Bepi-Colombo spacecraft when they were radially aligned and orbiting near 0.17 AU and 0.58 AU, respectively. PSP magnetic field observations are taken from the FIELDS fluxgate magnetometer (MAG) (Bale et al. 2016) and are averaged to 1-s cadence from their native 4 samples per cycle cadence (see also Alberti et al. 2020). BepiColombo magnetic field data are obtained by the fluxgate magnetometer on board the MPO spacecraft (Glassmeier et al. 2010; Heyner et al. 2021) with its boom already deployed during cruise.

The interplanetary magnetic field data are analyzed in the RTN coordinate system in which R is pointing toward the Sun, T tangential to the spacecraft orbit, and N normal to the R-T plane (Fränz & Harper 2002). The time interval corresponding to the radial alignment is the same as in Alberti et al. (2022) and it is reported in Figure 1. As shown in Alberti et al. (2022)
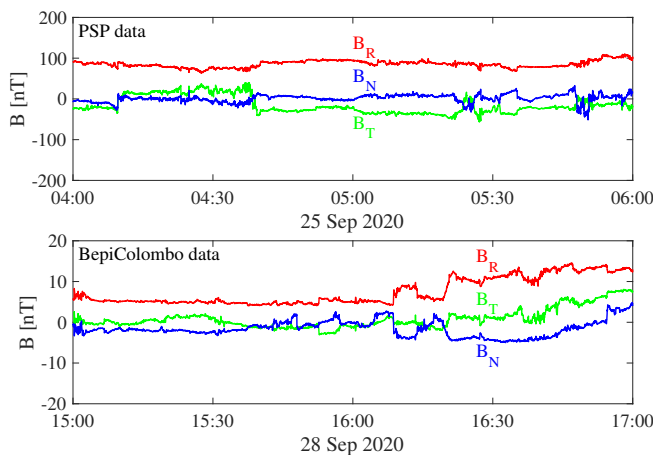

Fig. 1. The interplanetary magnetic field data in the RTN reference frame: 25 September 2020 04:00-06:00 UT for Parker Solar Probe (a) and 28 September 2020 15:00-17:00 UT for BepiColombo (b).

the radial alignment between PSP and BepiColombo occurred for the time intervals 04:00-06:00 UT on 25 September, 2020, for PSP, and 15:00-17:00 UT on 28 September, 2020, for Bepi-Colombo. These two intervals have been obtained by assuming that a plasma parcel is rigidly transported by the solar wind from PSP to BepiColombo orbit. This clearly depends on the measured solar wind speed at PSP orbit, thus determining the effective travel time to reach BepiColombo orbit. As shown in (Fig. 1 of Alberti et al. 2022) since V_{SW} = 240 km/s and the spacecraft separation is Δr = 0.4775 au, the corresponding travel time τ is about 3.5 days.

The method of reduced magnetic helicity σ_m is used in the data analysis, constructed as (cf., Matthaeus and Smith 1981;

Matthaeus et al. 1982; Narita et al. 2009; Brandenburg et al. 2011; Narita 2022)

$$\sigma_m = \frac{k_R h_m}{E_m} \tag{1}$$

$$= \frac{\langle b_T^* b_N - b_N^* b_T \rangle}{\langle b_R^2 + b_T^2 + b_N^2 \rangle}, \tag{2}$$

where k_R is the radial component of the wavevector (from the Sun), h_m is the one-component magnetic helicity density in the spectral domain defined as

$$h_m = -i \frac{k_R}{k^2} \left(\langle b_T^* b_N \rangle - \langle b_N^* b_T \rangle \right) \tag{3}$$

and $E_m = \langle b_R^2 + b_T^2 + b_N^2 \rangle$ is the spectral energy estimated by the trace of the spectral matrix of the fluctuating magnetic field, and $*$ refers to the complex conjugate. The angular bracket $\langle \cdots \rangle$ denotes the averaging over different realizations (over the time sub-intervals in our work). The essence of the reduced helicity is to extract the information on the spatial field rotation sense around the direction of interest (the radial direction from the Sun in our case) in a dimensionless form by normalizing to the fluctuation energy. Eq. (2) highlights the physical meaning of the magnetic helicity: it is a measure of the asymmetric part of the covariance matrix. These are the missing elements when only estimating the spectral density, corresponding to the diagonal elements of the covariance matrix.

The observational studies show that the helicity values can be both positive and negative (around the flow direction), and even oscillate between the two signs in a wider range of frequencies. The helicity magnitude falls off as a function of the frequencies. Naively speaking, when one applies the inertial-range energy spectrum for isotropic, homogeneous turbulence, to the off-diagonal element of the spectral matrix, i.e., $|b_T^\dagger b_N| \sim k^{-5/3}$, the helicity magnitude falls off as $|h_m| \sim k^{-8/3}$ which is steeper than the inertial-range energy spectrum.

The Fourier spectra are computed via the standard fast Fourier transform (FFT) method performed using a windowed approach consisting of a discrete spheroidal sequence with a time-bandwidth product $N_W = 4$ (Percival and Walden 1993). The spectra are then smoothed by means of convolution with a Papoulis window function with a bandwidth Δf such that $\Delta f / f = 7\%$ (Percival and Walden 1993; Podesta and Gary 2011). This operation ensures to evaluate the smoothed spectrum over a uniformly-spaced frequency grid matching that used to compute the spectrum.

2.2. Results

Figure 2 reports the helicity spectrum $h_m(f_{sc})$ at both PSP and BepiColombo locations. An interesting feature emerging by comparing both locations is a clear different scaling exponent. While close to the Sun $h_m \sim f^{-5/2}$, far away (around 0.6 au) it behaves as $h_m \sim f^{-8/3}$. These features seem to be in agreement with recent works (e.g., Chen et al. 2020; Alberti et al. 2020) who firstly noted that the energy spectral exponent, i.e., that associated with the symmetric part of the covariance matrix, moves from −3/2 to −5/3 when moving away from the Sun, with the transition occurring near 0.4 au. By simple dimensional arguments we can easily find that our observations on the reduced helicity match those in the power spectral density behavior. This is, at our knowledge, the first time we observe this feature.

By looking at the behavior of the normalized helicity σ_m (see Figure 3) other interesting features seem to emerge. First of all,
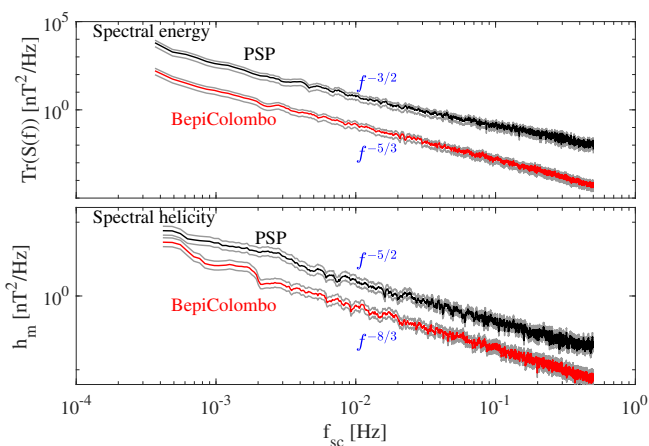
Fig. 2. (Upper panel) The trace of the Fourier power spectral densities (PSDs) for PSP (black line) and BepiColombo (red line) orbits. The PSD at PSP orbit follows the Iroshnikov-Kraichnan scaling of MHD turbulence $f^{-3/2}$, while at BepiColombo orbit the Kolmogorov scaling of fluid turbulence $f^{-5/3}$ is observed. (Lower panel) The helicity spectrum h_m at both PSP (a) and BepiColombo (b) locations, respectively. h_m at PSP orbit follows a $f^{-5/2}$ power-law, while at BepiColombo orbit a $f^{-8/3}$ scaling is observed. The gray lines are the 95% confidence intervals for both panels.
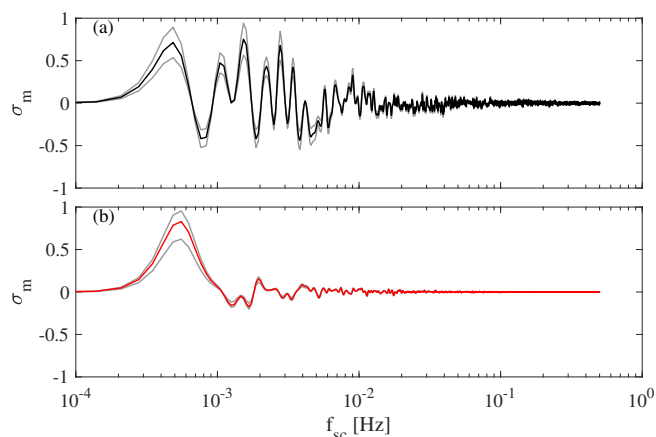

Fig. 3. The reduced helicity for (upper panel) PSP and (lower panel) BepiColombo. The gray lines are the 95% confidence intervals.

close to the Sun σ_m fluctuates between positive and negative values, while at BepiColombo orbit it seems to be almost positive. Secondly, approaching the inertial range break (around $f_{sc} \sim 0.1$-1 Hz) it seems that at PSP orbit larger fluctuations are found with respect to those at BepiColombo (almost zero). These findings both suggest that a common feature at 1 au that σ_m tends to non-zero in the ion-kinetic range (around 0.1 or 1 Hz) is not appearing. Furthermore, it was randomly oscillating around the zero mean at frequencies around 1 Hz, so from the view point of helicity study, we do not see any signature of kinetic Alfvén waves (KAWs) at both PSP and BepiColombo locations. There seem to be something at lower frequencies with non-zero helicity that might be the ion cyclotron wave (propagating parallel or antiparallel to the large-scale magnetic field) firstly predicted by Marsch and Tu (1990) using Helios particle data.

Looking from the lowest frequencies, the following features are obtained.

1. The reduced helicity reaches a peak of 70% positive polarization in the lowest frequency domain at about 5×10^{-4} Hz

at the both locations. This might represent a large-scale helical sense of the solar atmosphere or coronal field transported primarily by the solar wind advection. There is a moderate peak frequency shift from 5.0×10^{-4} Hz (PSP) to 5.5×10^{-4} Hz (BC), but the significance of the shift cannot be judged in the analyzed data resolution.

2. The reduce helicity exhibits larger fluctuations between positive values and negative values at PSP, reaching 40% negative polarization and 70% positive in the intermediate frequency range up to 10^{-2} Hz. In contrast, the reduce helicity shows only moderate fluctuations, below 20% polarization in the intermediate frequency range. Some wave activities are expected at PSP locations such as the excitation of ion-cyclotron mode (Marsch and Tu 1990). The Helios proton velocity distribution functions can be well fitted by the scenario of pitch angle scattering by the ion-cyclotron waves (Marsch and Tu 1990). The current analysis shows that the wave activity almost rests at the BC location.

3. The reduced helicity remains nearly zero-mean in the higher frequency range (approaching to 1 Hz). The oscillation is also moderate. This feature makes a marked difference from the reduced helicity profile observed at the Earth orbit (1 au) that the helicity shows a systematic trend and deviates from the zero-mean.

3. Conclusions and outlook

Though limited in the frequency range, the radial alignment event achieved by PSP and BC offers an opportunity of tracking the magnetic helicity in the plasma parcel in the inner heliosphere. The helicity spectra exhibit the features that the solar wind develops into turbulence by convecting large-scale helicity components on one hand and creating and annihilating helical wave components on the other hand. Excitation of waves can alter the helicity profile in the inner heliosphere. By comparing with the typical helicity spectra at a distance of 1 AU (that is, randomly oscillating helicity sign in the intermediate frequency range up to about 1 Hz), the helicity evolution approaches to an asymptotic state at the Venus orbit (about 0.7 AU) and beyond.

The PSP-BC radial alignment in the inner heliosphere extending from 0.17 AU to 0.58 AU enables us to track the evolution of the helical sense of magnetic field around the radial direction from the Sun. The reduced magnetic helicity shows three main features: (i) a coherent major peak (highly helical component) at the lowest frequency (at about 5×10^{-4} Hz) on the analyzed time interval, (ii) damping helicity oscillation in the intermediate frequencies (10^{-3} to 10^{-2} Hz) when observed at 0.58 AU, and (iii) a coherent non-helical component in the ion-kinetic range (frequencies $0.1 - 1$ Hz) at BepiColombo location (0.58 AU).

The reduced helicity at the Earth orbit often exhibits a different spectrum characterized by zero-mean, random oscillations at lower frequencies (where the MHD picture is valid) and a systematic trend to non-zero helicity at higher frequencies (the ion-kinetic range) interpreted as the sign of KAW excitation.

To conclude our work, a magnetic helicity evolution scenario is proposed as follows.

3.1. Large-scale helicity advection

The main novelty of our study is that the large-scale helicity is mainly transported by the solar wind advection. Indeed a coherence major peak at 5×10^{-4} Hz is observed both at PSP and Bepi-Colombo orbit, thus suggesting an underlying transport mecha-

nism primarily related to solar wind advection. This can be interpreted as a signature of processes related to solar wind heating and acceleration via linear resonance and instabilities in the solar corona that propagate through the inner heliosphere (e.g., Gary and Borovsky 2004; Podesta and Gary 2011). Thus, possible source of helicity in the solar atmosphere include instabilities, while the observed weak radial scaling of the helicity peak and frequency location could indicate waves are likely generated through in situ processes (Bowen et al. 2020).

3.2. Mid-frequency waves

The helicity sign shows systematic trend both in the positive and negative senses in the range 10^{-3} to 10^{-2} Hz with waves damped by the time when the solar wind reaches the BepiColombo orbit (about 0.58 AU). Based on our frequency resolution (1 Hz) we cannot explore the possibility of occurrence of ion-cyclotron or whistler waves, mainly centered in the 1-10 Hz range at PSP location (Bowen et al. 2020; Verniero et al. 2020). The observed damping of waves in the intermediate frequency range could be due to the interaction with the turbulent cascade. This scenario seems to be supported by the evolution of the nature of the inertial-range dissipation mechanisms at PSP and BepiColombo orbits (e.g., Alberti et al. 2022). Indeed, a different role of large and small field gradients could produce damping mechanisms in terms of helicity properties. While large field gradients are needed to dissipate energy via the turbulent cascade close to the Sun, small fluctuations are primarily responsible for the energy transfer rate far away. This reflects in large amplitude fluctuations in the reduced helicity at PSP with respect to those observed at BepiColombo. Thus, damping mechanisms could be searched in the interaction with inertial range physics (avalanching non-multiplicative vs. multiplicative processes, Alberti et al. 2022).

3.3. Ion-kinetic candidate waves

Short-wavelength or ion-kinetic waves, in the proper sense of Kinetic Alfvén Waves (KAWs), i.e., as deviation from MHD Alfvén waves, occurring at about the ion gyroradius r_{gi} (Narita et al. 2020), cannot be directly investigated due to our frequency resolution (Huang et al. (2020) reported the signature of the KAW in the range 2-26 Hz). Assuming that at these frequencies the linear-mode picture is valid, we can conjecture on the existence of some modes like (i) ion cyclotron mode changing into kinetic Alfvén mode, or (ii) whistler mode which splits into ion Bernstein modes, or (iii) slow mode with kinetic extension (e.g., Narita et al. 2020). Unfortunately, the mode(s) cannot be unambiguously identified, requiring a more dedicated analysis method which is beyond the scope of our study here.

Of course, the above scenario is drawn from one radial alignment event, and the question is valid as to its statistical significance. Yet, the scenario can be used as a reference model, and is useful in theoretical modeling of solar wind turbulence.

References

Alberti, T., Laurenza, M., Consolini, G., Milillo, A., Marcucci, M. F., Carbone, V., & Bale, S. D., 2020, Astrophys. J., 902, 84. doi:10.3847/1538-4357/abb3d2

Alberti, T., Milillo, A., Heyner, D., Hadid, L. Z., Auster, H.-U., Richter, I., & Narita, Y., 2022, Astrophys. J., 926, 174. doi:10.3847/1538-4357/ac478d

Bale, S. D., Goetz, K., Harvey, P. R., et al., 2016, Space Sci. Rev., 204, 49–82. doi:10.1007/s11214-016-0244-5

Biskamp, D., 2003, Magnetohydrodynamic Turbulence. Cambridge University Press, Cambridge. doi:10.1017/CBO9780511535222

Bowen, T. A., Mallet, A., Huang, J., Klein, K. G., Malaspina, D. M., Stevens, M., Bale, S. D., Bonnell, J. W., Case, A. W., Chandran, B. D. G., Chaston, C. C., Chen, C. H. K., Dudok de Wit, T., Goetz, K., Harvey, P. R., Howes, G. G., Kasper, J. C., Korreck, K. E., Larson, D., Livi, R., MacDowall, R. J., McManus, M. D., Pulupa, M., Verniero, J. L., & Whittlesey, P. Astrophys. J. Suppl., 246, 66. doi:10.3847/1538-4365/ab6c65

Brandenburg, A., Subramanian, K., Balogh, A., et al. 2011, ApJ, 734, 9. doi:10.1088/0004-637X/734/1/9

Chen, C. H. K., Bale, S. D., Bonnell, J. W., Borovikov, D., Bowen, T. A., Burgess, D., Case, A. W., Chandran, B. D. G., de Wit, T. Dudok, Goetz, K., Harvey, P. R., Kasper, J. C., Klein, K. G., Korreck, K. E., Larson, D., Livi, R., MacDowall, R. J., Malaspina, D. M., Mallet, A., McManus, M. D., Moncuquet, M., Pulupa, M., Stevens, M. L., & Whittlesey, P., 2020, Astrophys. J. Suppl. , 246, 53. doi:10.3847/1538-4365/ab60a3

Fränz, M. & Harper, D. 2002, Planet. Space Sci., 50, 217. doi:10.1016/S0032-0633(01)00119-2

Gary, S. P., & Borovsky, J. E., 2004, J. Geophys. Res., 109, A06105. doi:10.1029/2004JA010399

Glassmeier, K.-H., Auster, H.-U., Heyner, D., et al. 2010 Planet. Space Sci., 58,287–299. doi:10.1016/j.pss.2008.06.018

Heyner, D., Auster, H.-U., Fornaçon, K.-H., Carr, C., Richter, I., Mieth, J. Z. D., Kolhey, P., Exner, W., Motschmann, U., Baumjohann, W., Matsuoka, A., Magnes, W., Berghofer, G., Fischer, D., Plaschke, F., Nakamura, R., Narita, Y., Delva, M., Volwerk, M., Balogh, A., Dougherty, M., Horbury, T., Langlais, B., Mandea, M., Masters, A., Oliveira, J. S., Sánchez-Cano, B., Slavin, J. A., Vennerstrøm, S., Vogt, J., Wicht, J., & Glassmeier, K. -H., 2021, Space Sci. Rev., 217, 52. doi:10.1007/s11214-021-00822-x

Huang, S. Y., Zhang, J., Sahraoui, F., He, J. S., Yuan, Z. G. and Andrés, N., Hadid, L. Z., Deng, X. H., Jiang, K., Yu, L., Xiong, Q. Y., Wei, Y. Y., Xu, S. B., Bale, S. D., & Kasper, J. C., 2020, Astrophys. J. Lett., 897, L3. doi:10.3847/2041-8213/ab9abb

Leamon, R. J., Smith, C. W., Ness, N. F., Matthaeus, W. H., & Wong, H. K., 1998, J. Geophys. Res., 103, 4775–4788. doi:10.1029/97JA03394

Marsch, E., & Tu, C. -Y., 1990, J. Geophys. Res., 95, 821–8229. doi:10.1029/JA095iA06p08211

Matthaeus, W. H. and Smith, C. W., 1981, Phys. Rev. A, 24, 2135–2144. doi:10.1103/PhysRevA.24.2135

Matthaeus, W. H., and Goldstein, M. L., 1982, J. Geophys. Res., 87, 6011–6028. doi:10.1029/JA087iA08p06011

Matthaeus, W. H., Goldstein, M. L., Smith, C., 1982, Phys. Rev. Lett., 48, 1256–1259. doi:10.1103/PhysRevLett.48.1256.

Narita, Y., Kleindienst, G., & Glassmeier, K. -H., 2009, Ann. Geophys., 27, 3967–3976. doi:10.5194/angeo-27-3967-2009

Narita, Y., Roberts, O. W., Vörös, Z., and Hoshino, M., 2020, Front. Physics, 8, 166. doi:10.3389/fphy.2020.00166

Narita, Y., 2022, in AGU book "Helicities in Geophysics, Astrophysics and Beyond", ed. Rodion, S., Valery, N., Kuzanyan, K., & Yokoi, N., American Geophysical Union, John Wiley & Sons.

Percival, D. B., Walden, A. T., 1993, Spectral Analysis for Physical Applications, Cambridge University Press, Cambridge, doi:10.1017/CBO9780511622762

Podesta, J. J., & Gary, S. P., 2011, Astrophys. J., 734, 15. doi:10.1088/0004-637X/734/1/15

Podesta, J. J., 2013, Solar Phys., 286, 529–548. doi:10.1007/s11207-013-0258-z

Smith, C. W., 2003, Adv. Space Res., 32, 1971–1980. doi:10.1016/S0273-1177(03)90635-1

Taulor, G. I., 1938, Proc. Roy. Soc. London Ser. A, 164, 476–490. doi:10.1098/rspa.1938.0032

Telloni, D., Bruno, R., Trenchi, L., 2015, Astrophys. J., 805, 46. doi:10.1088/0004-637X/805/1/46

Verniero, J. L., Larson, D. E., Livi, R., Rahmati, A., McManus, M. D., Pyakurel, P. Sharma, Klein, K. G., Bowen, T. A., Bonnell, J. W., Alterman, B. L., Whittlesey, P. L., Malaspina, David M., Bale, S. D., Kasper, J. C., Case, A. W., Goetz, K., Harvey, P. R., Korreck, K. E., MacDowall, R. J., Pulupa, M., Stevens, M. L., de Wit, T. Dudok, 2020, Astrophys. J. Suppl., 248, 5. doi:10.3847/1538-4365/ab86af